УДК 2.2.15
DOI: 10.26102/2310-6018/2023.43.4.005

Performance analysis of underwater visible light reflecting system

Mohammad Furqan Ali✉, Dushantha Nalin K. Jayakody

School of Computer Science and Robotics, Tomsk Polytechnic University, Tomsk, the Russian Federation

Abstract. Underwater visible light communication (UVLC) has become a promising wireless signaling approach towards the 5G and 5G beyond (5GB) wireless networks. The depth-dependent photophysical characteristics of water such as pressure, density, temperature, and salinity fluctuations lead to the changes in the refraction index and turbulence of water. The channel turbulence is a bottleneck for optical signaling in aqueous mediums, especially in oceans; it also causes malfunctions in transceivers because of signal bias or pointing error. The paper examines the performance of the reflecting node as part of underwater optical communication system operating in visible light. Based on the experimental data obtained in the Southern Indian Ocean, the outage outcomes and bit-error-rate (BER) performances are considered. The performance metrics for the proposed system model are obtained under weak-turbulence channel conditions within Pulse-Amplitude Modulation (PAM) scheme. Additionally, the authors analytically present the closed-form expression for outage probability and a tight asymptotic expression for BER performance at high signal-to-noise (SNR) ratio that offers helpful insights into the influence of the medium on channel parameters and the system as a whole. The simulation results demonstrate operational capacity of the underwater communication system model.

Keywords: underwater wireless communication (UWC), underwater visible light communication (UVLC), underwater reflecting communication, underwater weak-turbulence, diver to diver communication (D2D), reflective semiconductor optical amplifier (RSOA).

Acknowledgments: this research was funded as part of the Competitiveness Enhancement Program of National Research Tomsk Polytechnic University, Russia.

For citation: Ali M. Furqan, Dushantha Nalin K. Jayakody. Performance analysis of underwater visible light reflecting system. *Modeling, Optimization, and Information Technology*. 2023;11(4). URL: https://moitvivt.ru/ru/journal/pdf?id=1402 DOI: 10.26102/2310-6018/2023.43.4.005

Анализ производительности подводной системы отражения видимого света

Мохаммад Фуркан Али✉, Душанта Налин К. Джаякоди

Инженерная школа информационных технологий и робототехники, Национальный исследовательский Томский политехнический университет, Томск, Российская Федерация

Резюме. Подводная связь в видимом свете привлекла большое внимание к анализу беспроводных оптических сигналов для следующего поколения беспроводных операторов связи, соответствующих стандарту 5G и выше (5GB). Зависящие от глубины физико-химические свойства воды, такие как колебания температуры, давления, плотности и солености, формируют разные значения показателей преломления, а также турбулентности воды. Канальная турбулентность является узким местом для распространения оптических сигналов в водных средах, особенно в океанах, а также причиной некорректной работы приемопередатчиков по причине смещения сигнала или ошибки наведения. Настоящее исследование посвящено анализу производительности отражающего узла в системе подводной оптической связи, работающей в видимом свете. На основе экспериментальных данных, полученных при изучении океана, рассматриваются показатели отказоустойчивости и коэффициенты битовых ошибок при

передаче сигнала. В предлагаемой модели системы показатели производительности получены в условиях канала слабой турбулентности в рамках схемы амплитудно-импульсной модуляции. Кроме того, аналитически выведено выражение в закрытой форме для характеристики простоя и точное асимптотическое выражение для коэффициента битовых ошибок при высоком отношении сигнал-шум, из которого можно извлечь данные о влиянии среды на параметры канала связи и системы в целом. Результаты моделирования показывают работоспособность модели системы подводной связи в видимом свете.

Ключевые слова: подводная беспроводная связь (UWC), подводная связь в видимом свете (UVLC), подводная отражающая связь, подводная турбулентность, общение между пловцами (D2D), отражательный полупроводниковый оптический усилитель (RSOA).

Благодарности: работа выполнена в рамках Программы повышения конкурентоспособности Национального исследовательского Томского политехнического университета, Россия.

Для цитирования: Али М. Фуркан, Душанта Налин К. Джаякоди. Анализ производительности подводной системы отражения видимого света. *Моделирование, оптимизация и информационные технологии*. 2023;11(4). URL: https://moitvivt.ru/ru/journal/pdf?id=1402 DOI: 10.26102/2310-6018/2023.43.4.005 (на англ.).

Introduction

The water reservoirs are highly critical channels for signal propagation, especially deep sea and oceans. Oceans are the most viable and mixed water reservoirs, and the necessity is to unveil the mysteries of these boisterous sectors. The oceans are widely used for defense, transportation, and commercial applications. Therefore, there is a need to establish a multiple communication system or divers for oceanographic data collection in marine-biological operations. In the last decades, underwater visible light communication (UVLC) has received the attention of the most suitable wireless carrier candidates in aqueous mediums and is highly in demand to deploy for various underwater applications [1]. However, the optical signal propagation through laser or LED covers moderate underwater ranges because of the large-scale fading due to high turbidity and physio-chemical properties of water [2]. Consequently, throughout this study, we are proposing a system model by utilizing an amplified modulating retro-reflector (AMMR) for long-range communication. It is noteworthy that this AMMR is based on a reflective semiconductor optical amplifier (RSOA), which is widely used for optical signal transmission in multiple directions and reliable communication among nodes in terms of robust outcomes. However, the RSOA is used in two ways (up-link and down-link) communication by deploying single light sources [3]. The fundamental advantages of RSOA deployment are the reflectance and signal modulation simultaneously. On the other hand, modulating retro-reflectors (MRRs) are the main substitutions for two ways of optical communication in reflecting optical signals. Additionally, the MRRs are also the assembly of a retro-reflector and a modulator to reflect modulated optical signals and receive by transceivers [4]. The main function of MRR components is subsequently divided as total internal reflector, phase and liquid crystal modulation, etc. As, with all above mentioned facts, it seems that RSOA has superiority over MRR because of the amplification, modulation, and signal reflectance simultaneously.

In the literature, limited works examine optical signal reflectance; they are mostly focused on point-point (P2P) and relay-based underwater communication. For instance, in [5], the authors have proposed an unmanned aerial vehicle (UAV) for ground communication through an MRR-based FSO link. The authors have investigated the closed-form expression in terms of the probability distribution function (PDF) and cumulative density function (CDF) for obtaining outage probability and bit-error-rate (BER) performance [5]. In another similar research [6], the authors derived the closed-form expression to the performance metrics by

utilizing MRR retro-reflector under gamma-gamma fading distribution. Although, in [7], the authors have developed an MRR communication link using optical orbital angular momentum (OAM) scheme for high-order coding. Therefore, there is a gap in the existing literature and a lack of enough contribution of UVLC performance under weak-turbulence channel conditions. The main purpose of this study is to propose a novel underwater optical communication system by utilizing water properties. Therefore, it has become necessary to develop a retro-reflector underwater visible light communication (RR-UVLC) system for various underwater applications. However, the water properties such as density, pressure, temperature, and salinity are directly responsible for changes in the refractive index. The refractive index contributes to the signal intensity fluctuations for underwater optical communication. An experimental investigation of statistical distribution and intensity fluctuations for communication under different channel conditions is proposed in [8]. Moreover, a transmit laser selection for diver-to-diver UVLC link is also proposed in [9]. It seems that the VLC signal reflector is minimally used in underwater applications. In our study, we are proposing a system model depicted in Figure 1, where one diver communicates with the other diver through signal reflectance phenomenon in the presence of an RSOA retro-reflector.

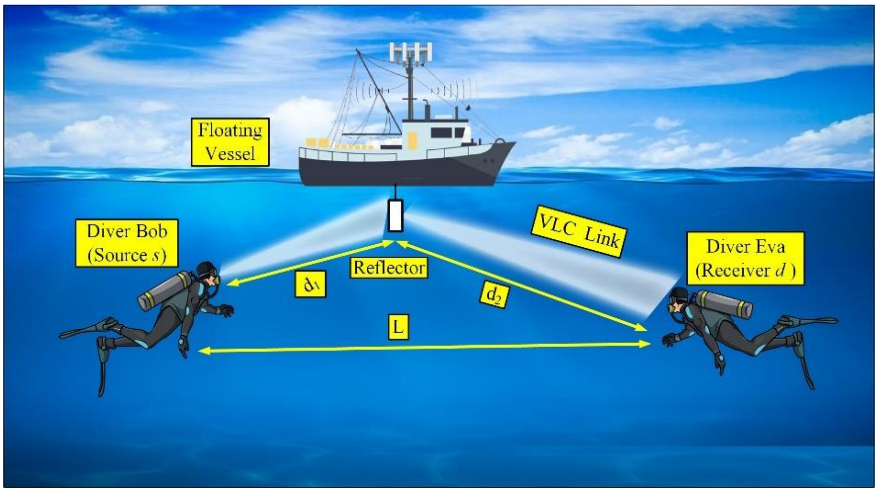

Figure 1 – Proposed system model where the divers communicate through the reflector optical beam under weak turbulence channel conditions

Рисунок 1 – Модель предлагаемой системы, в которой водолазы осуществляют связь через отражающий оптический луч в условиях слабого турбулентного канала

Motivated by this research, the proposed system model provides less complexity of signal modulation and demodulation than existing relayed system models in the literature. Additionally, in relayed communication, the relay has an extra cost of encoding/decoding and amplifies channel noise. That can be the reason for reducing the optical system efficiency. Due to this, we utilize the RSOA retro-reflector in underwater communication for high reliability, better efficiency, and a low-cost communication setup. In the authors' consideration, very limited works are available, where an RSOA reflector is utilized under weak-turbulence channel conditions with higher modulation techniques such as pulse amplitude modulation (PAM). The following contributions are highlighted in this study as follows:

1. The proposed UVLC system is applicable for signal-reflecting scenarios within the different types of shallow waters for underwater exploration and various applications.

2. A closed-form mathematical expression of outage probability is offered along with a tight asymptotic expression for BER performance at high SNR (infinite SNR $\gamma \to \infty$) modes.

3. In this research paper, the performance of the UVLC system is obtained under weak turbulence channel conditions by utilizing RSOA in the ocean for real-time monitoring of

floating nodes and divers. The performances are based on averaging physio-chemical properties every three months (quarterly) in regards to less complexity of the channel.

4. The investigated system is subjected to the lognormal distribution fading under higher modulation PAM scheme. In this study, the analysis and performance metrics are formulated under high SNR $\gamma \to \infty$ channel conditions.

5. In consideration of optical beam, absorption and scattering are crucial to optimize the system outcomes [10]. Therefore, the absorption and scattering coefficients have been accounted for and affect the simulation results.

The rest of the study is structured as follows: the design of UVLC is discussed in section II. However, the influence of channel conditions on the system performances under weak-turbulence channel conditions is considered. Due to this, the lognormal turbulence distribution for the scintillation index under the plane wave model is mentioned. The BER and outage performance under the PAM scheme following intensity modulation and direct detection (IM/DD) technique are analytically obtained through section III. The simulation results are verified based on the numerical results in section IV. Finally, section V provides a summary of the research as a whole.

System model

In this paper, we are considering a diver Bob (as a source node *s*) that transmits the optical signals towards the diver Eva (as a receiver node *d*) through an RSOA reflector *r* under weak turbulence channel conditions as depicted in Figure 1. It is noteworthy that a chunk of the transmitted signal is absorbed or scattered in another direction, and the remaining part of the optical beam is amplified and received at the receiver end. It is also assumed that the system is modeled under the PAM modulation scheme. In consideration of this work, the signal transmission is dependent on apparent optical properties (AoPs). However, these properties are related to the physical parameters of experimental assemblies, such as the conversion efficiency (η) and photo-detector responsivity (R), optical intensity (I), and channel conditions. Therefore, the received signals at the receiver can be written as follows:

$$y = R\eta(I + I_b)x + n = R\eta Ix + n. \quad (1)$$

In (1), the light intensities as I and I_b are associated with the beam propagation, and the interference of I_b can be effectively filtered by the optical filters which are out of the scope of this study [11]. The variable x is the information transmission symbol along with the additive white Gaussian noise (AWGN) n with zero-mean and σ^2 variance as presented. Emphasizing the instantaneous electrical SNR is given as $\gamma = R^2\eta^2|I|^2/\sigma^2$, which depends on the physical parameters and channel noise [11]. The average instantaneous SNR (μ) is given as $\mu = (R\eta E|I|)^2/E(\sigma)^2$. Additionally, optimizing the instantaneous SNR taking normalization of I as $E[I] = 1$, the average SNR could be written as $\mu = \gamma/I^2$.

For a diverse explanation of this study, it considers that the optical irradiance I is impaired by channel turbulence and the nature of the water. Due to this, we are taking the different assumptions for extinction coefficient $c(\lambda)$ for distinct water qualities. The combined influences of the optical beam are designed as the turbulence I_T and signal path-loss coefficient I_l. The coefficient of path-loss is modeled by Beer-Lambert's law ($I_l = exp\{-c(\lambda)L)\}$), where L is the distance between nodes. The path-loss I_l is deterministic and depends on the nature of water types. Therefore, the combined normalized channel fading irradiance is written as $I = I_T I_l$.

Generally, the light intensity experiences fading in terms of absorption, scattering, and scintillation index (SI), which contributes to the turbulence. Under weak turbulence channel conditions, the distribution-fading coefficient of turbulence I_T follows a lognormal distribution.

In the existing literature, the PDF of log irradiance intensity of channel conditions is given as [12]:

$$f_{I_T}(I_T) = \frac{1}{\sqrt{2\pi\sigma_T^2 I_T^2}} \exp\left(-\frac{\left(\ln(I_T) - \mu_T\right)^2}{2\sigma_T^2} \right), \tag{2}$$

where $\sigma_T^2 = 4\sigma_x^2$ and $\mu_T = 2\mu_x$ are denoted as variance and mean, respectively [9]. It is noted that an optical beam experiences irradiance fluctuation or SI within the underwater environment, which is formally known as optical turbulence. The SI rises with increasing Rytov variance which is defined by (6). It is noteworthy that the SI is large-scale (α) and small-scale (β) turbulent eddies dependent. Moreover, the corresponding α and β parameters depend on water temperature, pressure, density, and salinity and are given as [13]:

$$\alpha \cong \left[\exp\left(\frac{0.49\sigma_{I_x}^2}{\left(1+1.11\sigma_{I_x}^{12/5}\right)^{7/6}} \right) - 1 \right]^{-1}, \tag{3}$$

$$\beta \cong \left[\exp\left(\frac{0.51\sigma_{I_y}^2}{\left(1+0.69\sigma_{I_y}^{12/5}\right)^{7/6}} \right) - 1 \right]^{-1}. \tag{4}$$

The combined influence by suspended particles of SI is given as follows:

$$\sigma_T^2 = \left(1+\frac{1}{\alpha}\right)\left(1+\frac{1}{\beta}\right) - 1 = \frac{1}{\alpha} + \frac{1}{\beta} + \frac{1}{\alpha\beta}. \tag{5}$$

In this study, the determination of the physio-chemical properties of water follows the assumption of the plane wave model in (3) and (4). The Rytov variance $\sigma_{I_{x,y}}$ is derived in Appendix-A and given as follows [14]:

$$\sigma_{I_{x,y}}^2 = \frac{2\pi k_0^2 d_0 \alpha^2 \chi_T}{\varepsilon^{1/3}\omega^2} \int_0^1 \int_0^\infty \frac{1}{\kappa^{8/3}} \left\{ 1 - \cos\left[\frac{\kappa^2 d_0 \xi}{k_0} \right] \right\} \times \left[1 + C_1 (\kappa\eta)^{2/3} \right] \left(\omega^2 \exp(-A_T\delta) + d_r \exp(-A_S\delta) - \omega(d_r+1)\exp(-A_{TS}\delta) \right) d\kappa d\zeta \tag{6}$$

In (6), the parameters are enlisted in Table 1.

Table 1– Variables used in equation (6)
Таблица 1 – Переменные, используемые в уравнении (6)

Wave number	$k_0 = 2\pi / \lambda$
Link distance	d_0
The magnitude of spatial frequency	κ

Table 1 (extended)
Таблица 1 (продолжение)

Wave number	$k_0 = 2\pi / \lambda$
The relative strength of temperature and salinity	ω
Normalize distance	ξ
Kolmogorov micro-scale length	η
Constants	C_0, C_1
Eddy diffusivity ratio	d_r.
Kolmogorov micro-scale length	η
Dissipation rate of mean squared temperature and salinity	χ_T, χ_S

Analytical expressions and performance analysis

Throughout this section, the analytical work is summarized as well as the outage probability and BER performances under weak turbulence channel conditions are obtained. The combined influence of underwater turbulence and misalignment phenomena is considered throughout this study.

The outage performance of the system

The combined channel conditions under weak turbulence and pointing errors conditions are derived in Appendix-B and can be written as follows [15, (5)]:

$$f_\gamma(\gamma) = \frac{\zeta^2 \gamma^{\left(\zeta^2-1\right)}}{\left(A_0 \bar{\gamma}\right)^{\zeta^2}} \int_{\gamma/A_0\bar{\gamma}}^{\infty} t^{-\zeta^2} f(t) dt, \tag{7}$$

where the pointing error, collected energy fraction, and instantaneous SNR are denoted by ζ, A_0, and γ, respectively. However, the term $t = \gamma / \bar{\gamma}$ has been defined along with the average SNR $\bar{\gamma}$. Further, the substitution of t parameters is utilized in (2) as $f(t) = \frac{1}{2t\sqrt{2\pi\sigma_X^2}} \exp\left(-\frac{\left(\ln(t) - 2\mu_X^2\right)}{8\sigma_X^2}\right)$, and replaced in (7). Then, having some mathematical manipulation and utilizing hyperbolic tangential lognormal (HTLN) distribution by integration, the PDF can be given as follows [16, (13)]:

$$f_\gamma(\gamma) = \frac{e^{2\phi}\zeta^2 \gamma^{\psi-1}}{(A_0\bar{\gamma})^{\psi}} G_{1+\psi,1+\psi}^{1+\psi,1}\left[\frac{e^{2\phi}\zeta^2}{(A_0\bar{\gamma})^{\psi}\gamma^{\psi}}\middle| \begin{matrix} -1, \frac{i-\psi+\zeta^2-1}{\psi} \\ \frac{i-\psi+\zeta^2-2}{\psi}, 0 \end{matrix}\right], \tag{8}$$

where $i = 1, 2, ...\psi$; furthermore, for obtaining the cumulative distribution function (CDF) of PDF by utilizing the properties of Wolfram-Mathematica [17, (26)], the CDF given as

$$F_\gamma(\gamma) = \frac{e^{2\phi}\zeta^2}{\psi(A_0\bar{\gamma})^{\psi}} \gamma^{\psi} G_{1+\psi,1+\psi}^{1,1+\psi}\left[\frac{e^{2\phi}}{(A_0\bar{\gamma})^{\psi}}\middle| \begin{matrix} \frac{i-\psi}{\psi}, -1, \frac{i-\psi+\zeta^2}{\psi} \\ \frac{i-\psi+\zeta^2}{\psi}, 0, \frac{i-\psi-1}{\psi} \end{matrix}\right]. \tag{9}$$

It should be emphasized that the CDF could be used for the combined influence of transceiver misalignment and turbulence channel conditions. However, the CDF expression of the system within a non-pointing error scenario could be written to obtain the outage probability (P_{out}) of the proposed system. It is noteworthy that the E2E SNR should be less than or equal to the threshold SNR, which is further written as;

$$P_{out} = P_r(\gamma \le \gamma_{th}) = F_{\gamma}(\gamma_{th}). \tag{10}$$

Therefore, the analytical expression of the outage probability for the proposed system is derived as

$$P_{out} = \frac{e^{2\varphi}\zeta^2\gamma_{th}^{\psi}}{\psi(A_0\bar{\gamma})^{\psi}} G_{1+\psi,1+\psi}^{1,1+\psi}\left[\frac{e^{2\phi}}{(A_0\bar{\gamma})^{\psi}}\middle| \begin{matrix}\frac{i-\psi}{\psi}, \frac{i-\psi+\zeta^2}{\psi} \\ \frac{i-\psi+\zeta^2}{\psi}, 0, \frac{i-\psi-1}{\psi}\end{matrix}\right]. \tag{11}$$

Error-rate performance analysis

Throughout this section, the analytical expressions of BER are presented. This study considers the VLC system under the assumption of a PAM modulation scheme. However, the BER can be written as

$$\overline{BER} = \int_0^{\infty} \Gamma erfc\sqrt{\Omega\bar{\mu}I_T^2}\, f_{I_T}(I_T) dI_T \,. \tag{12}$$

In (12), *Γ=(M − 1)/(M log2(M))*, average *SNR* ($\bar{\mu}$), and *Ω=3/(2(M−1)(2M−1))* are represented, respectively. Therefore, the average BER over the PDF of I_T can be written by replacing (2) with (12) as follows:

$$\overline{BER} = \frac{\Gamma}{\sqrt{2\pi\sigma_T^2}} \int_0^{\infty} \frac{1}{I_T} \exp\left(-\frac{(\ln(I_T)-\mu_T)^2}{2\sigma_T^2}\right) \sqrt{\Omega\bar{\mu}I_T^2}\, dI_T \,. \tag{13}$$

Utilizing the change of integration variable $x = \left(\mu_T - \ln(I_T)/\sqrt{2}\sigma_T\right)$, we can obtain (14) from (13) as

$$\overline{BER} = \frac{\Gamma}{\sqrt{\pi}} \int_{-\infty}^{\infty} \exp(-x^2) erfc\left(\sqrt{\Omega\bar{\mu}}\exp(\mu_T - \sqrt{2}\sigma_T x)\right) dx \,. \tag{14}$$

Furthermore, using the approximation used in [18] as $erfc(x) \cong \frac{1}{6}\exp(-x^2) + \frac{1}{2}\exp\left(-\frac{4x^2}{3}\right)$, we obtain (15) from (14) as follows:

$$\overline{BER} = \frac{\Gamma}{2\sqrt{\pi}} \int_{-\infty}^{\infty} \exp\left\{\bar{\mu}\underbrace{\left(-\Omega\exp(2\mu_T)\exp(-2\sqrt{2}\sigma_T) - \frac{x^2}{\bar{\mu}}\right)}_{I_1}\right\} + \exp\left\{\bar{\mu}\underbrace{\left(-\frac{4\Omega}{3}\exp(2\mu_T)\exp(-2\sqrt{2}\sigma_T) - \frac{x^2}{\bar{\mu}}\right)}_{I_2}\right\} dx \,. \tag{15}$$

If x_{I_1} and x_{I_2} are the solution of derivatives $I_1^{'} = 0$ and $I_2^{'} = 0$, we obtain (16) and (17) as follows:

$$x_{I_1} = \frac{1}{2\sqrt{2}\sigma_T} W(4\bar{\mu}\sigma_T^2 \Omega \exp(2\mu_T)), \tag{16}$$

$$x_{I_2} = \frac{1}{2\sqrt{2}\sigma_T} W(\frac{16}{3}\bar{\mu}\sigma_T^2 \Omega \exp(2\mu_T)). \tag{17}$$

In (16) and (17), W(.) is denoted as the Lambert-W function [19]. Additionally, the second derivative of x_{I1} and x_{I2}, and $I_1^{"}$, $I_2^{"}$ can be replaced as in (18) and (19), which could be given as:

$$I_1^{"} = -8\sigma^2 \Omega \exp(2\mu_T) \exp(-2\sqrt{2}\sigma x) - \frac{2}{\bar{\mu}}, \tag{18}$$

$$I_2^{"} = -\frac{32}{3}\sigma^2 \Omega \exp(2\mu_T) \exp(-2\sqrt{2}\sigma x) - \frac{2}{\bar{\mu}}. \tag{19}$$

The BER for the investigated system could be defined by utilizing the method of Laplace integration as

$$\overline{BER} = \frac{\Gamma}{\sqrt{2\bar{\mu}}} \left[\frac{\exp(\bar{\mu} I(x_{I_1}))}{3\sqrt{|I_1^{"}(x_{I_1})|}} + \frac{\exp(\bar{\mu} I(x_{I_2}))}{\sqrt{|I_2^{"}(x_{I_2})|}} \right]. \tag{20}$$

To expand (20) by replacing the expression (16)-(19) in (20), we obtained (21) as the overall system BER performance of this study. In the following expression (21), we are considering the asymptotically BER performance at high SNR $\gamma \to \infty$ modes. However, the decreasing BER over the lognormal fading channel does not cover the finite value of instantaneous SNR. Therefore, for high SNR values, we utilize the expression as $exp(\bar{\mu} I_1) \gg exp(\bar{\mu} I_1)$. As a result, the asymptotic BER is obtained through the expression (22)

$$\overline{BER} \approx \frac{\Gamma \exp\left[-\bar{\mu}\Omega \exp(2\mu_T - B) - \frac{B^2}{8\sigma_T^2} \right]}{\sqrt{\left(144\bar{\mu}\sigma_T^2 \Omega \exp\left(2\mu_T - B\right) + 36\right)}} + \frac{\Gamma \exp\left[-\frac{4}{3}\bar{\mu}\Omega \exp\left(2\mu_T - \frac{16B}{3}\right) - \frac{32B^2}{9\sigma_T^2} \right]}{\sqrt{\left(\frac{64}{3}\bar{\mu}\sigma_T^2 \Omega \exp\left(2\mu_T - \frac{16B}{3}\right) + 4\right)}}, \tag{21}$$

$$\overline{BER} \approx \frac{\Gamma \exp\left[-\bar{\mu}\Omega \exp(2\mu_T - B) - \frac{B^2}{8\sigma_T^2} \right]}{\sqrt{\left(144\bar{\mu}\sigma_T^2 \Omega \exp\left(2\mu_T - B\right) + 36\right)}}, \tag{22}$$

where the parameter B is defined as $B = W\left(4\bar{\mu}\sigma_T^2 \Omega \exp(2\mu_T - B) + 36\right)$.

Numerical results

This section validates the analytical work and presents the E2E performance of the investigated system. In this study, the distance between transceivers *L=25m* is kept fixed. Unless, otherwise, we have used the given experimental data in the Southern Indian Ocean (SIO) up to *100m* depth. For the simulation results, we calculated σ_T^2 at different depths, temperatures, and salinity availability. This study limits the data up to 60*m* depth from the sea

surface. In this study, the green spectrum wavelength $\lambda=532nm$ is used to simulate the results for signal transmission.

The outage probability performance of the system is depicted in Figure 2 under varying threshold SNR conditions. It is clearly seen that with rising threshold SNR the system performance decreases. The best outage performance is obtained at $\gamma_{th}=2dBm$. It should be noted that the outage probability is simulated by utilizing the expression (11) while the temperature, salinity, and depth in terms of small (α) and large-scale (β) factors are averaging for the whole year.

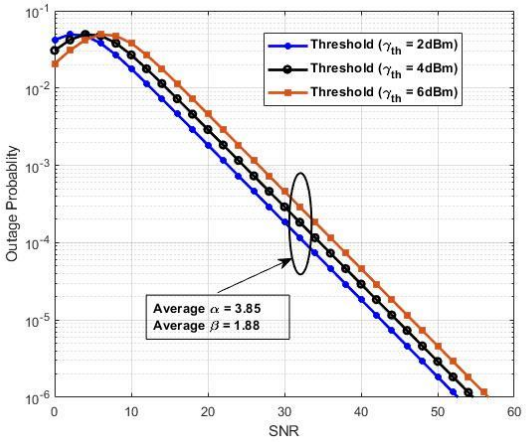

Figure 2 – Outage performance of the system under varying threshold SNR conditions with the average α and β particles for the whole year in the clear ocean water

Рисунок 2 – Характеристики отказов системы при изменении порогового SNR при средних значениях α и β частиц за весь год в прозрачной океанской воде

In Figure 3, we obtain the BER performance for varying channel conditions by utilizing equation (21). The BER performances are obtained based on averaging SI (σ_T) in each three months of the year. The SI $\sigma_T$is calculated based on experimentally recorded temperature, salinity, and depth of the water as in [20]. The optimum performance is obtained in the first three months (quarter) of the year while the worst is during the third quarter at a fixed vertical distance of *5m*. The most interesting phenomenon could be seen during the fourth quarter of the year, which is quite close to the first quarter. The first and fourth quarters are very close and have almost similar performances because of the variation of the water temperature and salinity rise during the end of the year (October to December). The performances in Figure 2 are quite close to the first quarter (beginning of the year as January to March). The first and fourth quarters are very close and have similar performances because of the variation of the water temperature and salinity rise during the end and in starting of the year. It seems that the salinity and temperature are effective signal-fading factors for optical beam propagation in aqueous mediums. Therefore, the authors obtained the performance metrics based on the absorption and scattering phenomena by using (21). We have considered the ocean as a clear ocean medium with extinction coefficient $c(\lambda) = 0.15$ in this study.

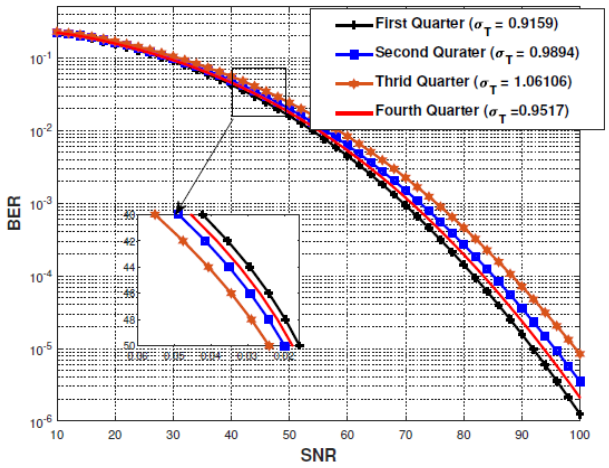

Figure 3 – BER performances obtained in SIO with varying average scintillation index (SI) along with fixed depth of the setup and fixed extinction coefficient of clear ocean water
Рисунок 3 – Характеристики BER, полученные в SIO при изменении среднего сцинтилляционного индекса (SI) при фиксированной глубине установки и фиксированном коэффициенте экстинкции чистой океанской воды

Another important scenario of this study is to obtain the BER performance under asymptotic SNR conditions. In Figure 4, we have obtained the asymptotic BER performance under weak turbulence channel conditions by simulating (22). Following the same approach as in Figure 3, the asymptotic performances are also obtained based on the averaging SI during the whole year. In Figure 4, the effect of SI in the first and fourth quarters also have a similar performance because of varying water physio-chemical properties while the poorest performances are obtained in the third quarter of the year 2016.

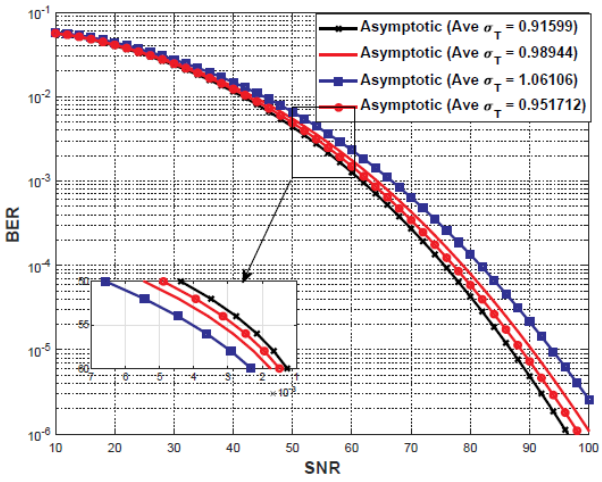

Figure 4 – Asymptotic BER performances obtained by using fixed vertical distance
Рисунок 4 – Асимптотические характеристики BER, полученные при использовании фиксированного вертикального расстояния

It is challenging to transmit signals on varying physiochemical properties of water. Due to this, the BER performances are obtained based on the varying temperature and salinity by using (21). In Figure 5, the performances are depicted at varying water properties, and it is noted that the best performance is achieved at the temperature and salinity $T = 6.99$ and $S = 31.55$ *PSU*, respectively. The dissipation rate of turbulence of kinetic energy per unit $\varepsilon = 10^{-2}$,

and the dissipation rate of mean-squared temperature χ_T =10^{-4} are taken with the fixed distance between communication nodes. So far, the worst performance is depicted at *S = 30.9 PSU*.

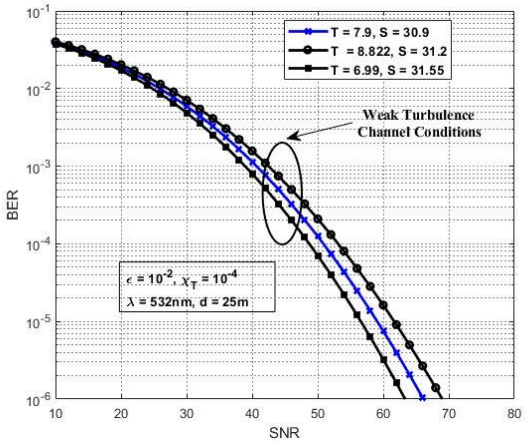

Figure 5 – BER performances obtained in SIO at varying temperatures and salinity with the communication depth fixed in the clear ocean water

Рисунок 5 – Характеристики BER, полученные в SIO при различных температурах и солености, где глубина связи поддерживается фиксированной в прозрачной океанской воде

The modulation schemes also play a significant role in the design of reflective UVLC system. The M-ary PAM modulation scheme is being used to transmit the optical signals. In this study, the performances under the PAM scheme are compared with the On-Off-Keying (OOK) modulation scheme. In Figure 6, the variation and comparison with OOK are depicted as the fixed vertical distance *d = 42.13m*, temperature *T = 8.006^{0}C*, salinity *S = 30.897 PSU*, and SI σ_T *= 0.4758*. The OOK modulation scheme shows superiority because of its simplicity rather than higher modulation. In Figure 6, it is depicted that higher modulation techniques show poorer performances within underwater channels. If targeting the performance as 10^{-4}, the OOK scheme achieves at *43.5dB* while 2-PAM and 4-PAM are achieved at *51dB* and *63.5dB*, respectively.

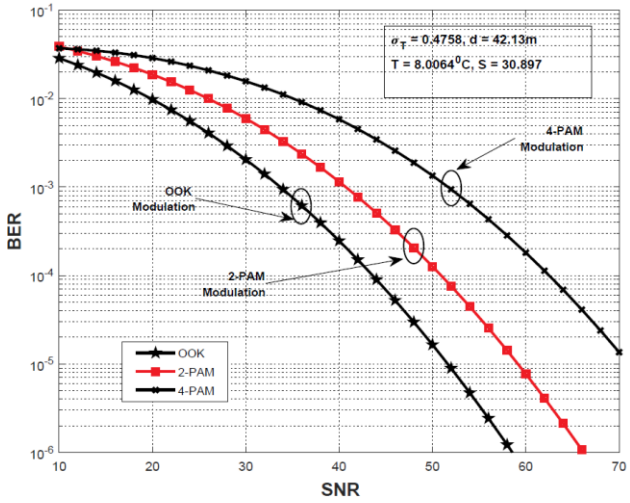

Figure 6 – An asymptotic BER performances obtained in SIO by utilizing the tight closed form with varying different distances

Рисунок 6 – Асимптотические характеристики BER, полученные в SIO с помощью жесткой замкнутой формы при варьировании различных расстояний

Conclusion

This research paper proposes an RSOA reflector-based UVLC system model in the Southern Indian Ocean (SIO), where the source node transmits the signal toward the receiver through an amplified reflector. The proposed system model is designed for the exploration of shallow water, especially for underwater diving. The experimental data under the weak turbulence channel conditions in shallow water is examined in this study. The signal attenuation coefficient for clear ocean water is also considered and applied to different aqueous mediums. The asymptotic and closed-form expressions for overall system performance are analytically investigated throughout this study. It would be interesting to extend this study to more detailed observation within the Southern Indian Ocean for the sake of high-speed and reliable communication within 5G and beyond (5GB) networks.

Appendix-A

According to Nikishov underwater optical turbulence (UOT), the spatial power spectrum of turbulent fluctuation of the seawater refraction index is given as follows [21]:

$$E_n(\kappa) = \frac{1}{4\pi\kappa^2\sqrt[3]{\varepsilon\kappa^5}}\chi_n C_0\left[1+C_1(\kappa\eta)^{2/3}\right]\phi(\kappa,\omega) \quad . \tag{23}$$

In (23), the κ is the magnitude of the spatial frequency, ε is the dissipation rate of turbulent kinetic energy per unit mass of fluid, and C_0, and C_1 are the constants, respectively. The parameter η is defined as the Kolmogorov microscale length, which is further given as $\eta = \sqrt[4]{\frac{\upsilon^3}{\varepsilon}}$, where the kinematic viscosity is defined by v. However, the dissipation rate of the mean-squared refractive index χ_T can be written as

$$\chi_n = \alpha^2\chi_T + \beta^2\chi_S - 2\alpha\beta\chi_{TS} \quad . \tag{24}$$

In (24), the factors α and β are denoted as the thermal expansion coefficient and the saline contraction coefficients. Further, the dissipation rate of mean-squared temperature and salinity along with the correlation coefficient are denoted as χ_T, χ_S, and χ_{TS}. More explicitly, these parameters are further written as follows:

$$\chi_T = K_T\left(\frac{dT_0}{dz}\right)^2 , \tag{25}$$

$$\chi_S = K_S\left(\frac{dS_0}{dz}\right)^2 , \tag{26}$$

$$\chi_{TS} = \frac{K_T+K_S}{2}\left(\frac{dT_0}{dz}\right)\left(\frac{dS_0}{dz}\right) . \tag{27}$$

In (25) and (26), the coefficient K_T and K_S denote the eddy diffusivity of salinity and temperature, respectively. (5) can be modified by replacing the values of K_T and K_S in (27) as follows:

$$\chi_{TS} = \frac{1}{2}\left[\left(\frac{dS_0/dz}{dT_0/dz}\right)\chi_T + \left(\frac{dT_0/dz}{dS_0/dz}\right)\chi_S\right]. \quad (28)$$

Throughout the (23), the parameter $\phi(\kappa,\omega)$ is given as follows:

$$\phi(\kappa,\omega) = \frac{1}{\omega^2 - (1-d_r)\omega + d_r} \times\left(\omega^2 \exp\left(-\frac{C_0\delta}{P_T C_1^2}\right) + d_r \exp\left(-\frac{C_0\delta}{P_S C_1^2}\right) - \omega(d_r+1)\exp\left(-\frac{C_0\delta}{2P_{TS}C_1^2}\right)\right). \quad (29)$$

However, in (29), P_T and P_S denote the Prandtl numbers for temperature and salinity, while the parameter δ is defined as follows:

$$\delta = 1.5C_1^2(\kappa\eta)^{4/3} + C_1^3(\kappa\eta)^2. \quad (30)$$

Furthermore, the Prandtl number is given in the form of kinematic viscosity υ and the molecular diffusivity of the temperature and salinity as D_T and D_S. Therefore, the Prandtl numbers can be written as $P_T = \upsilon / D_T$ and $P_s = \upsilon / D_S$. The relative strength of temperature and salinity fluctuation ω is defined as follows:

$$\omega = \frac{\alpha(dT_0/dz)}{\beta(dS_0/dz)}. \quad (31)$$

The ratio of K_T and K_S is called the diffusivity ratio $d_r = K_S / K_T$. Through (25) and (26). the value of eddy diffusivity salinity and temperature in diffusivity ratio is as follows:

$$\chi_S = d_r \frac{(dS_0/dz)^2}{(dT_0/dz)^2}\chi_T. \quad (32)$$

Utilizing the ω value from (31) and manipulating some mathematical calculation, we obtain (33) as follows;

$$\chi_S = d_r\left(\frac{\alpha}{2\beta\omega}\right)^2\chi_T. \quad (33)$$

Additionally, by replacing the values of K_T and K_S in (28) and implies in (31), we could obtain χ_{TS} as follows:

$$\chi_{TS} = \left(\frac{\alpha}{2\beta\omega}\right)\chi_T + \left(\frac{\beta\omega}{2\alpha}\right)\chi_S. \quad (34)$$

Further modification of (33) could be written in terms of diffusivity ratio by implementing (34), and it is obtained from (35) as follows:

$$\chi_{TS} = \left(\frac{\alpha}{2\beta\omega}\right)\chi_T(1+d_r). \quad (35)$$

The dissipation rate of the mean-squared refractive index (χ_n) is given as follows:

$$\chi_n = \frac{\alpha^2 \chi_T}{\omega^2}\left[\omega^2 - (1+d_r)\omega + d_r\right]. \tag{36}$$

Finally, the spectrum model of underwater optical turbulence could be obtained by replacing (29) and (36) into (23) as follows:

$$E_n(\kappa) = \frac{C_0}{4\pi\kappa^2}\left(\frac{\alpha^2\chi_T}{\omega^2\varepsilon^{1/3}\kappa^{5/3}}\right)\left[1+C_1(\kappa\eta)^{2/3}\right]$$
$$\times\left(\omega^2\exp\left(-\frac{C_0\delta}{P_T C_1^2}\right)+d_r\exp\left(-\frac{C_0\delta}{P_S C_1^2}\right)-\omega(d_r+1)\exp\left(-\frac{0.5C_0\delta}{P_{TS}C_1^2}\right)\right). \tag{37}$$

The assumption of the contribution of salinity and density variation is equal to the contribution of temperature to density variation, i.e. $d_r = 1$ and $\omega = 1$. Then (37) modifies as follows:

$$E_n(\kappa) = \frac{C_0}{4\pi\kappa^2}\left(\frac{\alpha^2\chi_T}{\varepsilon^{1/3}\kappa^{5/3}}\right)\left[1+C_1(\kappa\eta)^{2/3}\right]$$
$$\times\left(\exp\left(-\frac{C_0\delta}{P_T C_1^2}\right)+\exp\left(-\frac{C_0\delta}{P_S C_1^2}\right)-2\exp\left(-\frac{0.5C_0\delta}{P_{TS}C_1^2}\right)\right). \tag{38}$$

It is noteworthy that for spherical waves under the assumption of weak turbulence, the Rytov variance could be calculated by [22] as follows:

$$\sigma_{I_{x,y}}^2 = 8\pi^2 k_0^2 d_0 \int_0^1\int_0^\infty \kappa E_n(\kappa)\left\{1-\cos\left[\frac{d_0\kappa^2}{k_0}\left(\xi-\xi^2\right)\right]\right\}d\kappa d\xi. \tag{39}$$

The final expression of Rytov variance is obtained by replacing (38) into (39) as follows:

$$\sigma_{I_{x,y}}^2 = 2\pi k_0^2 d_0 C_0 \alpha^2 \frac{\chi_T}{\omega^2\varepsilon^{1/3}}\int_0^1\int_0^\infty \kappa^{-8/3}\left\{1-\cos\left[\frac{d_0\kappa^2}{k_0}\left(\xi-\xi^2\right)\right]\right\}$$
$$\times\left[1+C_1(\kappa\eta)^{2/3}\right]\left(\omega^2\exp\left(-\frac{C_0\delta}{P_T C_1^2}\right)+d_r\exp\left(-\frac{C_0\delta}{P_S C_1^2}\right)-\omega(d_r+1)\exp\left(-\frac{0.5C_0\delta}{P_{TS}C_1^2}\right)\right)d\kappa d\xi. \tag{40}$$

Appendix-B

The probability distribution function (PDF) of the pointing error for a random variable is given as [22]

$$f_\gamma(\gamma) = \frac{\zeta^2\gamma^{\zeta^2-1}}{\left(A_0^{\zeta^2}\bar{\gamma}\right)^{\zeta^2}}\int_{\frac{\gamma}{A_0}}^\infty \gamma^{-\zeta^2} f_\gamma(\gamma)d\gamma. \tag{41}$$

The combined effect of channel conditions as turbulence and pointing error has been taken into account. For more explicit integration, the expression (41) is written by replacing $t = \gamma/\bar{\gamma}$ as follows:

$$f_{\gamma}(\gamma)=\frac{\zeta^2\gamma^{\zeta^2-1}}{\left(A_0^{\zeta^2}\overline{\gamma}\right)^{\zeta^2}}\int\limits_{\frac{\gamma}{A_0\overline{\gamma}}}^{\infty}t^{-\zeta^2}f_{\gamma}(t)dt \quad . \tag{42}$$

The HTLN expression (2) is a lognormal distribution and forms lognormal into hyperbolic tangent distribution HTD. The cumulative distribution function (CDF) is given as [16]

$$\Phi(x)=Q\left(\frac{\mu_X-x}{\sqrt{2\sigma_X^2}}\right)=\frac{1}{2}+\frac{1}{2}\tanh(bx+a) \quad , \tag{43}$$

where *a* and *b* are the constants and substituting x with ln(t)/2 in (38) along with putting *tanh*, which yields

$$F(t)=\frac{\exp(2a)t^b}{(1+\exp(2a)t^b)^2} \quad . \tag{44}$$

We integrate the CDF equation of (44) to obtain the PDF as $f(t)=\frac{b\exp(2a)t^{b-1}}{(1+\exp(2a)t^b)^2}$.

Furthermore, we put the values of equation (44) into equation (7) to obtain the closed-form expression of analysis in this study.

REFERENCES

1. Elamassie M., Miramirkhani F., Uysal M. Channel modeling and performance characterization of underwater visible light communications. In: *2018 IEEE International Conference on Communications Workshops (ICC Workshops), Kansas City, MO, USA.* 2018. p. 1–5. DOI: 10.1109/ICCW.2018.8403731.
2. Zedini E., Oubei H.M., Kammoun A., Hamdi M., Ooi B.S., Alouini M.-S. Unified statistical channel model for turbulence-induced fading in underwater wireless optical communication systems. *IEEE Transactions on Communications.* 2019;67(4):2893‑2907. DOI: 10.1109/TCOMM.2019.2891542.
3. Chen J., Yu Z., Wang T., Liu Z., Gao S. High-speed modulating retro-reflectors with optical phase conjugation compensation. *Optics Communications*. 2022;507:127629. DOI: 10.1016/j.optcom.2021.127629.
4. Ziph-Schatzberg L., Bifano T., Cornelissen S., Stewart J., Bleier Z. Deformable mems mirror in secure optical communication system. In: *Proc. SPIE 7318, Micro- and Nanotechnology Sensors, Systems, and Applications, 73180T, 11 May 2009, Orlando, Florida, United States.* 2009. p. 190–201. DOI: 10.1117/12.818831.
5. Dabiri M.T., Rezaee M., Mohammadi L., Javaherian F., Yazdanian V., Hasna O., Uysal M. Modulating retroreflector based free space optical link for UAV-to-ground communications. *IEEE Transactions on Wireless Communications*. 2022;21(10):8631–8645. DOI: 10.1109/TWC.2022.3167945.
6. Li C., Liu H., Lin W., Yan B., Li S., Liu B. Performance analysis of modulating retro-reflector free space optical communication system over gamma-gamma fading channels. *Microwave and Optical Technology Letters*. 2022;64(3):609–615. DOI: 10.1002/mop.33140.

7. Zhang Z., Yin X., Cui X., Chang H., Xin X. Performance analysis of modulating retro-reflector link based on orbital angular momentum coding in underwater channels. *Optics Communications*. 2022;127903. DOI: 10.1016/j.optcom.2022.127903.
8. Jamali M.V., Khorramshahi P., Tashakori A., Chizari A., Shahsavari S., AbdollahRamezani S., Fazelian M., Bahrani S., Salehi J.A. Statistical distribution of intensity fluctuations for underwater wireless optical channels in the presence of air bubbles. In: *2016 Iran Workshop on Communication and Information Theory (IWCIT). IEEE, Tehran, Iran.* 2016. p. 1–6. DOI: 10.1109/IWCIT.2016.7491626.
9. Elamassie M., Al-Nahhal M., Kizilirmak R.C., Uysal M. Transmit laser selection for underwater visible light communication systems. In: *2019 IEEE 30th Annual International Symposium on Personal, Indoor, and Mobile Radio Communications (PIMRC), Istanbul, Turkey.* 2019. p. 1–6. DOI: 10.1109/PIMRC.2019.8904100.
10. Kaushal H., Kaddoum G. Underwater optical wireless communication. *IEEE access*. 2016;4:1518‑1547. DOI: 10.1109/ACCESS.2016.2552538.
11. Elamassie M., Uysal M. Vertical underwater VLC links over cascaded gamma-gamma turbulence channels with pointing errors. In: *IEEE International Black Sea Conference on Communications and Networking (BlackSeaCom), Sochi, Russia*. 2019. p. 1‑5. DOI: 10.1109/BlackSeaCom.2019.8812811.
12. Bhowal A., Kshetrimayum R.S. Performance analysis of one-and two-way relays for underwater optical wireless communications. *OSA Continuum*. 2018;1(4):1400–1413. DOI: 10.1364/OSAC.1.001400.
13. Ali M.F., Jayakody D.N.K., Garg S., Kaddoum G., Hossain M.S. Dual-hop mixed FSO-VLC underwater wireless communication link. *IEEE Transactions on Network and Service Management.* 2022;19(3):3105–3120. DOI: 10.1109/TNSM.2022.3181169.
14. Elamassie M., Uysal M., Baykal Y., Abdallah M., Qaraqe K. Effect of eddy diffusivity ratio on underwater optical scintillation index. *Journal of the Optical Society of America A.* 2017;34(11):1969–1973. DOI: 10.1364/JOSAA.34.001969.
15. Yang F., Cheng J., Tsiftsis T.A. Free-space optical communication with nonzero boresight pointing errors. *IEEE Transactions on Communications*. 2014;62(2);713–725. DOI: 10.1109/TCOMM.2014.010914.130249.
16. Ramavath P.N., Udupi S.A., Krishnan P. Co-operative RF-UWOC link performance over hyperbolic tangent log-normal distribution channel with pointing errors. *Optics Communications*. 2020;469:125774. DOI: 10.1016/j.optcom.2020.125774.
17. Adamchik V., Marichev O. The algorithm for calculating integrals of hypergeometric type functions and its realization in reduce system. In: *Proceedings of the international symposium on Symbolic and algebraic computation. ACM*. 1990. p. 212–224.
18. Chiani M., Dardari D., Simon M.K. New exponential bounds and approximations for the computation of error probability in fading channels. *IEEE Transactions on Wireless Communications*. 2003;2(4):840–845. DOI: 10.1109/TWC.2003.814350.
19. Belkic D. The Euler T and Lambert W functions in mechanistic radio-biological models with chemical kinetics for the repair of irradiated cells. *Journal of Mathematical Chemistry*. 2018;56(8):2133–2193. DOI: 10.1007/s10910-018-0932-3.

20. Argo floats, “Southern Indian Ocean”. URL: https://argo.ucsd.edu/. [accessed on 15.12.2021].
21. Nikishov V.V., Nikishov V.I. Spectrum of turbulent fluctuations of the sea-water refraction index. *International Journal of Fluid Mechanics Research*. 2000;27(1)82–98. DOI: 10.1615/InterJFluidMechRes.v27.i1.70.
22. Farid A.A., Hranilovic S. Outage capacity optimization for free-space optical links with pointing errors. *Journal of Lightwave Technology*. 2007;25(7):1702‑1710. DOI: 10.1109/JLT.2007.899174.

СПИСОК ИСТОЧНИКОВ

1. Elamassie M., Miramirkhani F., Uysal M. Channel modeling and performance characterization of underwater visible light communications. In: *2018 IEEE International Conference on Communications Workshops (ICC Workshops), Kansas City, MO, USA.* 2018. p. 1–5. DOI: 10.1109/ICCW.2018.8403731.
2. Zedini E., Oubei H.M., Kammoun A., Hamdi M., Ooi B.S., Alouini M.-S. Unified statistical channel model for turbulence-induced fading in underwater wireless optical communication systems. *IEEE Transactions on Communications.* 2019;67(4):2893‑2907. DOI: 10.1109/TCOMM.2019.2891542.
3. Chen J., Yu Z., Wang T., Liu Z., Gao S. High-speed modulating retro-reflectors with optical phase conjugation compensation. *Optics Communications*. 2022;507:127629. DOI: 10.1016/j.optcom.2021.127629.
4. Ziph-Schatzberg L., Bifano T., Cornelissen S., Stewart J., Bleier Z. Deformable mems mirror in secure optical communication system. In: *Proc. SPIE 7318, Micro- and Nanotechnology Sensors, Systems, and Applications, 73180T, 11 May 2009, Orlando, Florida, United States.* 2009. p. 190–201. DOI: 10.1117/12.818831.
5. Dabiri M.T., Rezaee M., Mohammadi L., Javaherian F., Yazdanian V., Hasna O., Uysal M. Modulating retroreflector based free space optical link for UAV-to-ground communications. *IEEE Transactions on Wireless Communications*. 2022;21(10):8631–8645. DOI: 10.1109/TWC.2022.3167945.
6. Li C., Liu H., Lin W., Yan B., Li S., Liu B. Performance analysis of modulating retro-reflector free space optical communication system over gamma-gamma fading channels. *Microwave and Optical Technology Letters*. 2022;64(3):609–615. DOI: 10.1002/mop.33140.
7. Zhang Z., Yin X., Cui X., Chang H., Xin X. Performance analysis of modulating retro-reflector link based on orbital angular momentum coding in underwater channels. *Optics Communications*. 2022;127903. DOI: 10.1016/j.optcom.2022.127903.
8. Jamali M.V., Khorramshahi P., Tashakori A., Chizari A., Shahsavari S., AbdollahRamezani S., Fazelian M., Bahrani S., Salehi J.A. Statistical distribution of intensity fluctuations for underwater wireless optical channels in the presence of air bubbles. In: *2016 Iran Workshop on Communication and Information Theory (IWCIT). IEEE, Tehran, Iran.* 2016. p. 1–6. DOI: 10.1109/IWCIT.2016.7491626.
9. Elamassie M., Al-Nahhal M., Kizilirmak R.C., Uysal M. Transmit laser selection for underwater visible light communication systems. In: *2019 IEEE 30th Annual*

International Symposium on Personal, Indoor, and Mobile Radio Communications (PIMRC), Istanbul, Turkey. 2019. p. 1–6. DOI: 10.1109/PIMRC.2019.8904100.

10. Kaushal H., Kaddoum G. Underwater optical wireless communication. *IEEE access*. 2016;4:1518‑1547. DOI: 10.1109/ACCESS.2016.2552538.
11. Elamassie M., Uysal M. Vertical underwater VLC links over cascaded gamma-gamma turbulence channels with pointing errors. In: *IEEE International Black Sea Conference on Communications and Networking (BlackSeaCom), Sochi, Russia*. 2019. p. 1‑5. DOI: 10.1109/BlackSeaCom.2019.8812811.
12. Bhowal A., Kshetrimayum R.S. Performance analysis of one-and two-way relays for underwater optical wireless communications. *OSA Continuum*. 2018;1(4):1400–1413. DOI: 10.1364/OSAC.1.001400.
13. Ali M.F., Jayakody D.N.K., Garg S., Kaddoum G., Hossain M.S. Dual-hop mixed FSO-VLC underwater wireless communication link. *IEEE Transactions on Network and Service Management*. 2022;19(3):3105–3120. DOI: 10.1109/TNSM.2022.3181169.
14. Elamassie M., Uysal M., Baykal Y., Abdallah M., Qaraqe K. Effect of eddy diffusivity ratio on underwater optical scintillation index. *Journal of the Optical Society of America A*. 2017;34(11):1969–1973. DOI: 10.1364/JOSAA.34.001969.
15. Yang F., Cheng J., Tsiftsis T.A. Free-space optical communication with nonzero boresight pointing errors. *IEEE Transactions on Communications*. 2014;62(2);713–725. DOI: 10.1109/TCOMM.2014.010914.130249.
16. Ramavath P.N., Udupi S.A., Krishnan P. Co-operative RF-UWOC link performance over hyperbolic tangent log-normal distribution channel with pointing errors. *Optics Communications*. 2020;469:125774. DOI: 10.1016/j.optcom.2020.125774.
17. Adamchik V., Marichev O. The algorithm for calculating integrals of hypergeometric type functions and its realization in reduce system. In: *Proceedings of the international symposium on Symbolic and algebraic computation. ACM*. 1990. p. 212–224.
18. Chiani M., Dardari D., Simon M.K. New exponential bounds and approximations for the computation of error probability in fading channels. *IEEE Transactions on Wireless Communications*. 2003;2(4):840–845. DOI: 10.1109/TWC.2003.814350.
19. Belkic D. The Euler T and Lambert W functions in mechanistic radio-biological models with chemical kinetics for the repair of irradiated cells. *Journal of Mathematical Chemistry*. 2018;56(8):2133–2193. DOI: 10.1007/s10910-018-0932-3.
20. Argo floats, “Southern Indian Ocean”. URL: https://argo.ucsd.edu/. [дата обращение: 15.12.2021].
21. Nikishov V.V., Nikishov V.I. Spectrum of turbulent fluctuations of the sea-water refraction index. *International Journal of Fluid Mechanics Research*. 2000;27(1)82–98. DOI: 10.1615/InterJFluidMechRes.v27.i1.70.
22. Farid A.A., Hranilovic S. Outage capacity optimization for free-space optical links with pointing errors. *Journal of Lightwave Technology*. 2007;25(7):1702‑1710. DOI: 10.1109/JLT.2007.899174.

ИНФОРМАЦИЯ ОБ АВТОРАХ / INFORMATION ABOUT THE AUTHORS

Али Мухаммад Фуркан, аспирант, ассистент, Томский политехнический университет, Томск, Российская Федерация
e-mail: ali89@tpu.ru
ORCID: 0000-0001-7602-0209

Ali Mohammad Furqan, Postgraduate Student, Assistant Lecturer, Tomsk Polytechnic University, Tomsk, the Russian Federation.

Душанта Налин К. Джаякоди, Ph.D., профессор, Томский политехнический университет, Российская Федерация.
e-mail: nalin@tpu.ru
ORCID: 0000-0002-7004-2930

Dushantha Nalin K. Jayakody, Ph.D., Professor, Tomsk Polytechnic University, the Russian Federation.

Статья поступила в редакцию 26.06.2023; одобрена после рецензирования 23.08.2023; принята к публикации 12.10.2023.

The article was submitted 26.06.2023; approved after reviewing 23.08.2023; accepted for publication 12.10.2023.